Journal of Hazardous Materials 276 (2014) 120–128

Contents lists available at ScienceDirect

Journal of Hazardous Materials

journal homepage: www.elsevier.com/locate/jhazmat

Morphology controlled bulk synthesis of disc-shaped WO_3 powder and evaluation of its photocatalytic activity for the degradation of phenols

M. Aslam[a], Iqbal M.I. Ismail[a,b], S. Chandrasekaran[a], A. Hameed[a,c,*]

[a] Centre of Excellence in Environmental Studies (CEES), King Abdulaziz University, Jeddah 21589, Saudi Arabia
[b] Chemistry Department, Faculty of Science, King Abdulaziz University, PO Box 80203, Jeddah 21589, Saudi Arabia
[c] National Centre for Physics, Quaid-e-Azam University, Islamabad 44000, Pakistan

HIGHLIGHTS

- User friendly procedure for the synthesis of disc-shaped WO_3.
- Superoxide anion radicals are the major contributors in photocatalytic degradation process.
- Electron withdrawing substituents facilitates the degradation process.
- Nitrite ions are converted to NO_2 gas in 2-nitophenol degradation.

GRAPHICAL ABSTRACT

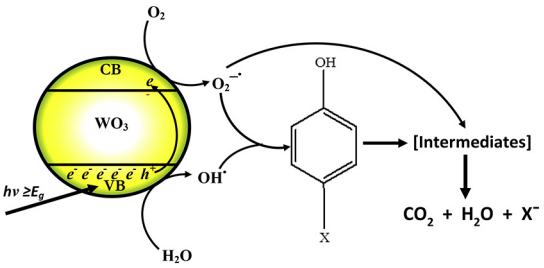

ARTICLE INFO

Article history:
Received 22 February 2014
Received in revised form 8 May 2014
Accepted 10 May 2014
Available online 16 May 2014

Keywords:
Disc-shaped WO_3
Sunlight photocatalysis
Phenol degradation

ABSTRACT

The surfactant assisted synthesis of disc-shaped WO_3 powder and its photocatalytic performance in sunlight exposure is reported. UV–vis DRS, XRD and FESEM characterized the synthesized WO_3. The synthesized powder exhibited a bandgap of ~2.55 eV with cubic lattice and high crystallinity. The photocatalytic activity of the synthesized WO_3 was examined for the degradation of phenol, resorcinol, 2-chlorophenol and 2-nitrophenol in complete spectrum and visible segment of sunlight. The highly efficient degradation/mineralization of 2-chloro and 2-nitrophenol compared to that of phenol and resorcinol, under identical experimental conditions, suggested the regulatory role of substituents attached to the aromatic ring in degradation/mineralization process. The time-scale HPLC degradation profiles, identification of intermediates by GC-MS and removal of organic carbon during the course of reaction were utilized to approximate the possible route of degradation/mineralization of phenolic substrates. The measurement of the anions released during the photocatalytic process was used to identify the nature of the major oxidants ($O_2^{\bullet-}$, $OH^{\bullet}$) and the possible interaction sites. A significant decrease in the photocatalytic activity of synthesized WO_3, ~50%, was observed in visible portion of sunlight however, a sustained activity was observed in the repeated exposures.

1. Introduction

Among the advanced oxidation technologies, heterogeneous photocatalysis, based on the illumination of semiconductor powders for the removal of organic contaminants from water, has gained particular interest [1–6]. TiO_2 is the most extensively

* Corresponding author at: King Abdulaziz University, Center of Excellence in Environmental Studies, PO Box 80216, Jeddah 21589, Saudi Arabia.
Tel.: +966506406684.
E-mail addresses: afmuhammad@kau.edu.sa, hameedch@yahoo.com (A. Hameed).

http://dx.doi.org/10.1016/j.jhazmat.2014.05.022
0304-3894/

studied photocatalyst for the decontamination of water, however owing to its absorption cross section in the UV region; it is unable to harvest the major portion of sunlight and can utilize only ≤5% of the total incident light radiation [7–23]. As ∼46% of the solar spectrum falls in the visible region, the wide spread economical application of this technology requires the development of photocatalysts capable of utilizing maximum portion of the sunlight with optimum activity. Among the existing photocatalysts, ZnO, having activity comparable to TiO_2, is the second most studied photocatalyst for water decontamination. Although better absorption cross-section in the sunlight; the wide bandgap, anodic dissolution and instability in highly acidic mediums, impose restriction on its use [24–27].

WO_3, with a bandgap between 2.4 and 2.8 eV, is a visible light responsive catalyst with stability in acidic conditions, which makes it a suitable choice for the photocatalytic degradation of organic pollutants under solar irradiation [28–30]. It has been reported that the particle morphology, that includes the shape and size, of a particular photocatalyst, significantly affects its photocatalytic activity [31]. Flower-like WO_3 assemblies, due to their specific hierarchical pores that served as the transport paths for light and reactants, exhibited higher visible-light photocatalytic activity than the particles. No significant decrease in the activity of these assemblies was observed after subsequent reuse confirming their stability and resistance towards photocorrosion [32]. The formation of disc-shaped WO_3 in the form of thin film at FTO substrate, using poly(ethylene glycol), is reported in the literature [33] however, no report regarding the bulk synthesis of disc-shaped WO_3 powder and its photocatalytic activity is available.

Phenol and its derivatives, because of their extensive use in chemical, petrochemical and pharmaceutical industries, is the major are among the most potential pollutants in the discharge from these industries. Owing to their chemical stability imparted by resonance, phenolic compounds are difficult to degrade by conventional water treatment technologies [34]. Another important aspect is their conversion into more toxic chlorinated compounds during the treatment for biological decontamination by chlorination.

Among the phenol derivatives, chloro and nitrophenols, being toxic and carcinogenic, are the most important pollutants [35–38]. Owing to their high solubility and chemical stability, nitro and chlorophenols derivatives are difficult to degrade [39,40]. The majority of the studies available on the degradation of phenol and its derivatives are carried out in the presence of TiO_2. Among the pure photocatalysts studied, WO_3 is the least studied for the degradation of phenol and its derivatives.

The current study comprises of morphology-controlled bulk synthesis, characterization and photocatalytic activity of the synthesized disc-shaped WO_3. The procedure adopted for the synthesis of bulk disc-shaped WO_3 is user friendly and entirely different from the one mentioned in the literature [33]. The photocatalytic performance of the synthesized powder was evaluated for the degradation of phenol, resorcinol, 2-chlorophenol (2-CP) and 2-nitrophenol (2-NP). In comparison to pure phenol, the possible role of the substituent (*electron donating* or *electron withdrawing*) attached to phenol derivatives on the degradation is discussed. The results obtained by various analytical tools (HPLC, TOC, IC and GCMS) are correlated to establish the mechanism of degradation.

2. Experimental details

The disc-shaped WO_3 powder was synthesized by chemical precipitation method [33] using sodium meta-tungstate (Analytical Grade, Sigma-Aldrich, USA) and Triton X-100 (Scintillation grade, purity >99%, BDH Chemicals Ltd., UK) as precursor for W^{6+} ions and surface active mediator respectively. Prior to use in the synthesis, the hydrated sodium meta tungstate was dried at a temperature of 120 °C in the vacuum oven (JSR, JSOF 100H) overnight. In a typical synthesis, 25 g of anhydrous sodium meta-tungstate (moisture content ≤0.01%), containing ∼18.6 g W^{6+} ions, was dissolved in ion free Milli-Q water under stirring. Triton X-100, 0.01% with respect to the weight of W^{6+} ions, was added to the precursor solution under vigorous stirring for optimum mixing. The metal/surfactant solution was acidified with the slow addition (7–10 drops/min) of 0.25 M HNO_3 under stirring at 2000 rpm (IKA Eurostar 20, Germany) until pH 2. The suspension was initially heated at 100 °C for 2 h and at an elevated temperature (250 °C) for 3 h. The suspension was aged overnight. The clear and colorless supernatant solution indicated the complete precipitation. The bulk of the precipitates were removed by filtration while the remaining precipitates were recovered by centrifugation. The precipitates were washed several times with hot water till the neutral pH of the filtrate. The residual surfactant was removed by successive washings with ethanol and acetone (50:50) mixture. The fine dry powder with shiny luster was initially dried in the oven at 120 °C and finally calcined at 450 °C.

A Perkin Elmer UV–vis diffuse reflectance spectrophotometer (DRS) equipped with integrating sphere was used to record the solid-state absorption and diffuse reflectance spectra of the synthesized WO_3 discs in 200–900 nm wavelength range. After applying Kubelka–Munk (K–M) transformation on $\%R$ values, the bandgap of the synthesized WO_3 was evaluated by plotting $(F(R) \times h\upsilon)^{1/2}$ versus $h\upsilon$ (photon energy, eV). The powder XRD patterns of synthesized disc-shaped WO_3 discs were recorded by Xpert X-ray powder diffractometer (Philips PW1398) with Cu $K\alpha$ radiation source from 20° to 80° (2θ) with a step time of 3 s and step size of 0.05°. Scherer's equation was applied on main reflections to evaluate the crystallite size of various phases. The morphology of the synthesized WO_3 was examined by field emission scanning electron microscope (FESEM) (JEOL JSM 6490-A).

The photocatalytic activity of disc-shaped WO_3 was evaluated by exposing the catalyst-phenolic solution suspension to sunlight. The optimized concentration of the individual phenolic substrate (phenol, resorcinol, 2-chlorophenol and 2-nitrophenol) was 30 ppm. All the experiments were performed with the catalyst loading of 300 mg by exposing 150 cm^3 of respective phenolic substrate (30 ppm). The optimization of catalyst loading was performed by exposing the catalyst-phenol suspensions (150 cm^3) having different catalyst loadings ranging from 50 to 500 mg for a fixed period of 30 min. Beyond 300 mg/150 cm^3 catalysts loading, the degradation curve lost linearity without significant change in the degradation therefore; all the experiments were performed with 300 mg catalyst loading. All the experiments were performed in the sunlight illumination of $1000 \pm 100 \times 10^2$ lx and fixed period of the daylight. The progress of degradation process was monitored by drawing the samples after every 30 min in the first 2 h and after 60 min in the next one hour. The catalyst was removed by using 0.20 μm Whatman syringe filters. The collected samples were analyzed by high performance liquid chromatography (HPLC), (SPD-20A, Shimadzu Corporation, Japan) using 60:40 Methanol-water mixture as solvent, c18 column and 284 nm wavelength. Thermo scientific, USA, ion chromatograph, Dionex (ICS-5000 + EG Eluent Generator), was used to measure the released ions during photocatalytic process. TOC-VCPH total carbon analyzer supplied by Shimadzu Corporation, Japan, measured total Organic Carbon (TOC) of the samples. Selected samples were analyzed by GC-MS (Shimadzu Corporation, Japan, Shimadzu-QP2010 Plus) equipped with RtX1 capillary column, for the identification of unknown compounds formed as intermediate during the mineralization process. Helium (He) was used as carrier gas. The experiments were performed in the dark to evaluate the interaction of catalyst and substrate. The direct interaction of photons, photolysis, with the phenolic substrates was also evaluated.

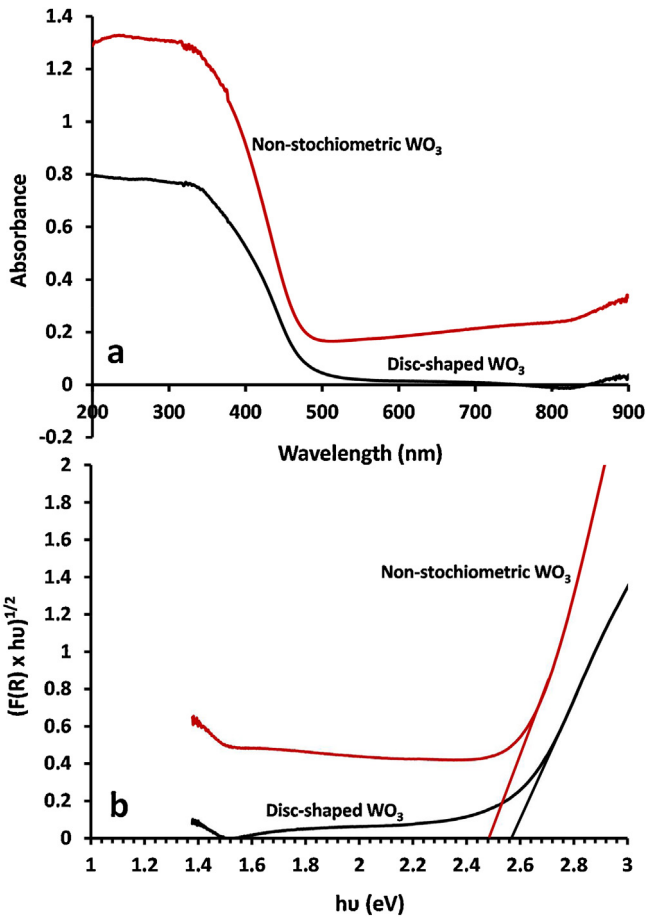

Fig. 1. (a) The comparison of solid state absorption spectra of synthesized disc-shaped stoichiometric WO_3 and non-stoichiometric WO_3: (b) the graphical evaluation of the bandgap obtained by extrapolating the plot between $(F(R) \times h\nu)^{1/2}$ versus photon energy $h\nu$ for disc-shaped and non-stoichiometric WO_3.

3. Results and discussion

3.1. Characterization of disc-shaped WO_3

The solid-state absorption and diffuse reflectance spectra of the disc shaped WO_3 in comparison with that of non-stoichiometric WO_3 are presented in Fig. 1a, where a strong absorption in 300–500 nm region was observed. The major electronic transitions in WO_3 appear due the transfer of electrons from the valance band (O 2p) to the conduction band (W, 4f). The sharp absorption edge in the absorption spectra indicates the well defined crystalline structure with high crystallinity. Also the smooth pattern of the absorption and DRS curves indicate the stochiometric WO_3 with fewer defects. In non-stoichiometry WO_3 the presence of W^{5+} states along with W^{6+} states, are the source of distortion and shifting of absorption bands (Fig. 1). As presented in Fig. 1b, the band edge of disc-shaped WO_3 was identified by plotting $F(\mathrm{R}) \times h\nu)^{1/2}$ versus $h\nu$. $F(R)$ was obtained by applying Kubelka–Munk transformation on reflectance data. The band edge of the disc shaped WO_3 appeared at ~2.55 eV which was in accordance with the literature values [28–30].

The FESEM images of disc shaped WO_3 powder at 7500× and 15,000× resolutions are presented in Fig. 2a and b, respectively, where the discs of various dimensions ranging from 200 to 800 nm ($L \times W$) can be observed. Interestingly the thickness of all the discs was uniform and ranged between 35 and 40 nm. The measurements of the disc dimension and thickness are presented in Fig. 2c and d.

The XRD patterns of disc-shaped WO_3 is presented in Fig. 3, where it can be observed that all the major reflections appear in the form of sharp peaks attributed to the high crystallinity of synthesized WO_3. The intense reflections at 2θ values of 23.14, 23.66, 24.45, 33.35, 41.70 and 44.9 corresponding to (0 0 2), (0 2 0), (2 0 0), (0 2 2), (2 0 2) and (1 2 3) *hkl* indices were matched with monoclinic WO_3 (JCPDS-43-1035) that represent highly crystalline defect free WO_3. The full scale XRD pattern showing all the major and minor reflections and their corresponding *hkl* indices are mentioned in Fig. 3. The average crystal size evaluated by applying Scherrer's equation on the most intense reflections was ~45.2 nm.

3.2. Photocatalytic degradation of phenol and its derivatives

The initiation of the photocatalytic degradation process requires the energy of incident photons equal to or higher than the bandgap of the photocatalyst. The bandgap excitation with the absorption of photons leads to the generation of highly oxidizing species in the aqueous medium that results in the photocatalytic degradation of organic contaminants. The oxidation of H_2O molecules by photogenerated holes (h^+) and reduction of dissolved oxygen by the conduction band electrons (e^-) results in the generation of hydroxyl ($OH^\bullet$) and superoxide anion radicals ($O_2^{\bullet-}$). As presented in the set of equations below, the aqueous phase photocatalytic processes are not limited to the formation of the above mentioned oxidizing species rather a chain of reactions is initiated generating a variety of charged neutral and ionic species [40].

$$WO_3 + h\nu \left(E \geq E_g\right) \rightarrow e^- + h^+ \quad (1)$$

$$H_2O + h^+ \rightarrow H_2O^+ \rightarrow HO^\bullet + H^+ \quad (2)$$

$$(O_2)_{ads} + e^- \rightarrow O_2^{\bullet-} \quad (3)$$

$$H_2O \rightarrow HO^- + H^+ \quad (4)$$

$$HO^- + h^+ \rightarrow HO^\bullet \quad (5)$$

$$O_2^{\bullet-} + H^+ \rightarrow HOO^\bullet \quad (6)$$

$$O_2^{\bullet-} + H^+ \rightarrow HO_2^\bullet \quad (7)$$

$$HO_2^\bullet + HO_2^\bullet \rightarrow H_2O_2 + 1/2O_2 \quad (8)$$

$$H_2O_2 + H^+ + e^- \rightarrow OH^\bullet + H_2O \quad (9)$$

For WO_3, the E_{vb} (+3.44 V) supports the oxidation of water (+1.23 V) by the photogenerated h^+ entities and the formation of hydroxyl radicals ($HO^\bullet$) (Eq. (2)), however, the E_{cb} (+0.74 V) completely negates the reduction of dissolved or adsorbed O_2 to superoxide anions ($O_2^{\bullet-}$) that requires the potential to be at −0.28 V (Eq. (3)). Regarding the role of photogenerated oxidizing species in the photocatalytic decontamination process, until recently, the hydroxyl radicals were regarded as the principal oxidants in photocatalytic degradation processes [18] however, lately [41] a limited role of hydroxyl radicals ($HO^\bullet$) in degradation processes has been reported and a pH dependent complex route for their formation has been proposed. The suggested route, involving H_2O_2, is as under.

$$HO_2^\bullet + HO_2^\bullet \rightarrow H_2O_2 + 1/2O_2 \quad (10)$$

$$H_2O_2 + H^+ + e^- \rightarrow OH^\bullet + H_2O \quad (11)$$

It has also been reported that the formation and existence of particular oxidizing species depends on various factors that include the potential of conduction band edge, pH_{ZPC} of the photocatalyst and pH of the medium itself. In general, the suitability of conduction band edge i.e. negative than −0.28 eV (the reduction potential of $O_2/O_2^{\bullet-}$ couple) and neutral or basic pH (≥7.0) supports the formation of the superoxide anion radicals whereas at lower pH values facilitates the formation of hydroxyl radicals ($HO^\bullet$) and H_2O_2

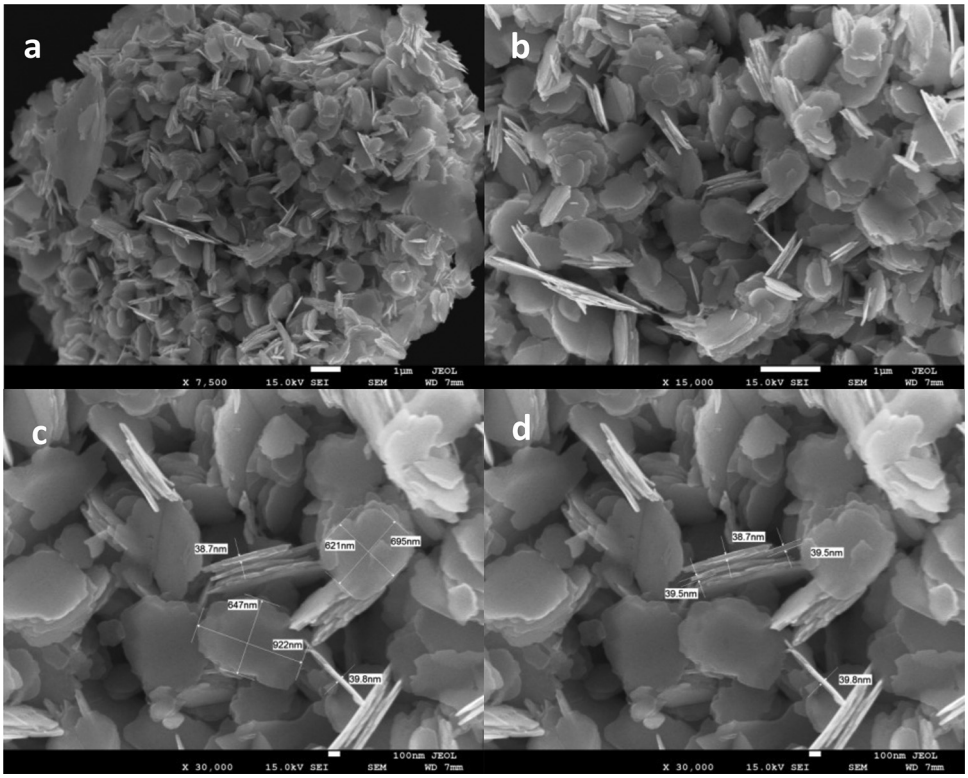

Fig. 2. The SEM profiles of synthesized WO_3 at various resolutions: (a) 7500× (b) 15,000× (c) measured dimensions of the discs at 30,000× and (d) measured thickness of the discs at 30,000×.

[41]. Based on the oxidation of adsorbed surface OH^- entities by photogenerated holes (h^+), at pH higher than the pH_{ZPC} of the photocatalyst, an alternative route for the formation of $OH^\bullet$ radicals is also suggested in the literature [42]. The proposed formation of hydroxyl is scarcely possible in the acidic medium.

$$OH^- + h^+ \rightarrow OH^\bullet \quad (12)$$

The HPLC profiles for the degradation of phenol, resorcinol, 2-chlorophenol (2-CP) and 2-nitrophenol (2-NP) are shown in Fig. 4a–d, where a significant variation in the time-scale degradation of each substrate accounting to a negligible decrease in the concentration of phenol and resorcinol and a rapid degradation of 2-CP and 2-NP was noticed. For phenol and resorcinol, owing to low degradation, fewer intermediates were formed whereas the degradation of 2-CP led to the accumulation of intermediates while for 2-NP, both the substrate and intermediates were removed simultaneously. Considering the peak heights as contemporary to the concentration of the substrates, the percentage degradation of phenol and its derivatives (resorcinol, 2-CP and 2-NP) was calculated on the basis of the decrease in peak heights.

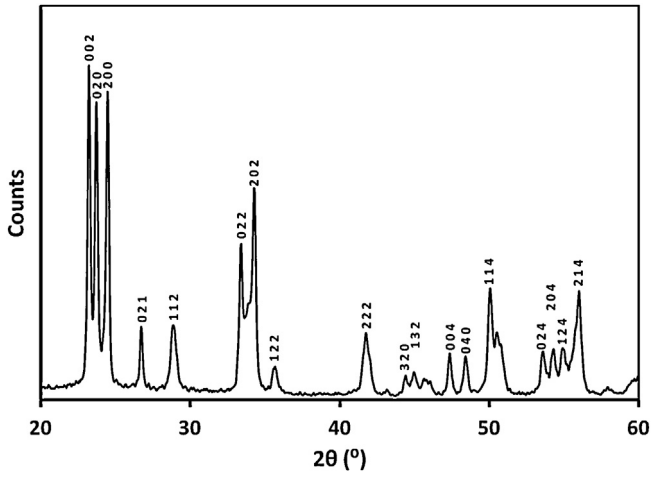

Fig. 3. The XRD profiles of synthesized WO_3 discs.

No significant decrease in the concentration of phenolic substrates in the dark due to adsorption and in sunlight exposure without catalyst because of direct photolysis was observed. Compared to ~1.85% for phenol and ~2.79% for resorcinol (Fig. 5a), in the initial 30 min of sun exposure, ~44% and ~62% degradation was observed for 2-CP and 2-NP, respectively. Both 2-CP and 2-NP was degraded almost completely (>98%) in 180 min of sunlight exposure whereas a decrease of ~8.4% and ~11.3% in the concentration of phenol and resorcinol was observed in the same period. The rates of degradation of the phenol and its derivatives were evaluated by using the kinetic model for pseudo first order reaction as detailed below.

$$C = C_o e^{-kt}$$

$$\ln\left(\frac{C_o}{C}\right) = kt$$

The values of rate constant (k), 0.0205 min^{-1} and 0.0270 min^{-1}, for 2-CP and 2-NP respectively, were significantly higher than that of 0.0007 min^{-1}, for phenol and resorcinol. The comparison of graphical evaluation of rate constants obtained by plotting $\ln(C_o/C)$ versus the sunlight exposure time (t) is presented in Fig. 5b.

A trend similar to that of degradation process was observed in the removal of total organic carbon i.e. mineralization (Fig. 6a).

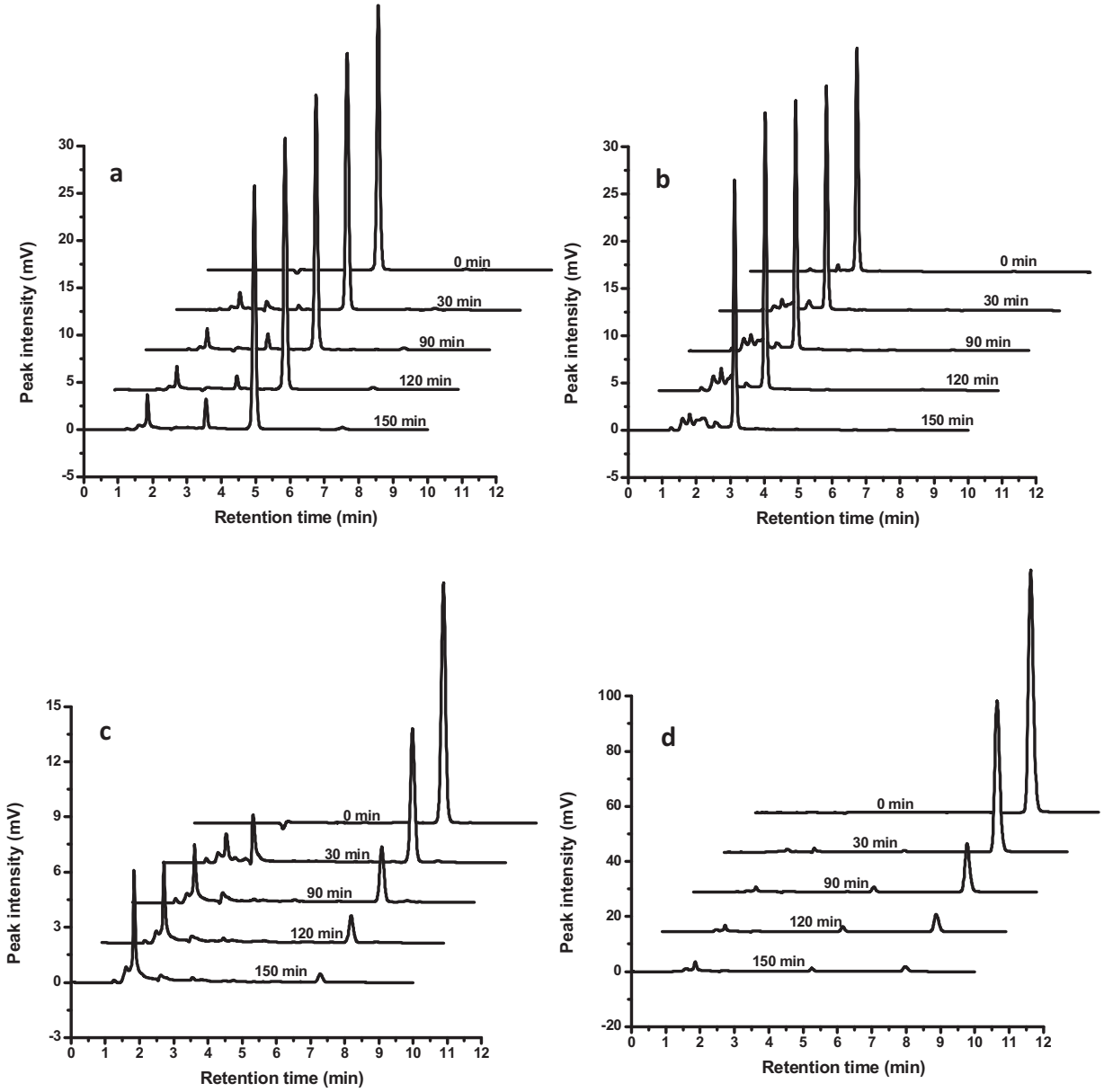

Fig. 4. The HPLC profiles for the degradation (a) phenol (b) resorcinol (c) 2-chlorophenol and (d) 2-nitrophenol in sunlight exposure at the catalyst loading of 300 mg suspended in 150 ml of the respective phenol solution.

Nevertheless, compared to percentage degradation, a low TOC removal was observed for all substrates. Compared to the percentage degradation of ~1.85%, ~2.79%, ~44% and ~62%, a TOC removal of ~0.5%, ~1.58%, ~34% and ~47% were observed for phenol, resorcinol, 2-CP and 2-NP respectively. Similarly, a low TOC removal rate (Fig. 6b), compared to that of degradation, was observed for all the substrates.

Theoretically, owing to the electrochemical potential of band edges especially the conduction band edge, WO_3 is completely unable to reduce the adsorbed/dissolved oxygen to superoxide anion radicals. However, the observed high degradation and mineralization of 2-CP and 2-NP suggested the involvement of superoxide anions in both the processes. Additionally, the sluggish degradation and mineralization of phenol and resorcinol also depicts that the majority oxidizing species that are produced under illumination are charged in nature and unable to attack electron rich resonance stabilized phenol and resorcinol. Also the rapid degradation of 2-CP and 2-NP whereas, the low degradation of resorcinol proposed that the presence of chloro and nitro groups facilitates while hydroxyl group retard the degradation process.

The observations discussed above suggest that besides the suitability of conduction band edge for the reduction of O_2 (dissolved or adsorbed), some alternative mechanism for the delivery of photogenerated e_{cb}^- to adsorbed/dissolved O_2 also prevails. During the photocatalytic degradation experiments, it was noticeable that the color of WO_3 powder changes from yellow to greenish with the absorption of photons. The observation was similar to that observed in our previous studies [43–46]. WO_3 is well known for its photo-chromic properties and mostly exists in slightly distorted monoclinic structure composed of WO_6 octahedra arranged in edge sharing configuration [47]. The stochiometric arrangement in which all the tungsten atoms possess 6+ oxidation states imparts yellow color to WO_3. In the sunlight exposure, the electronic transitions initiated by

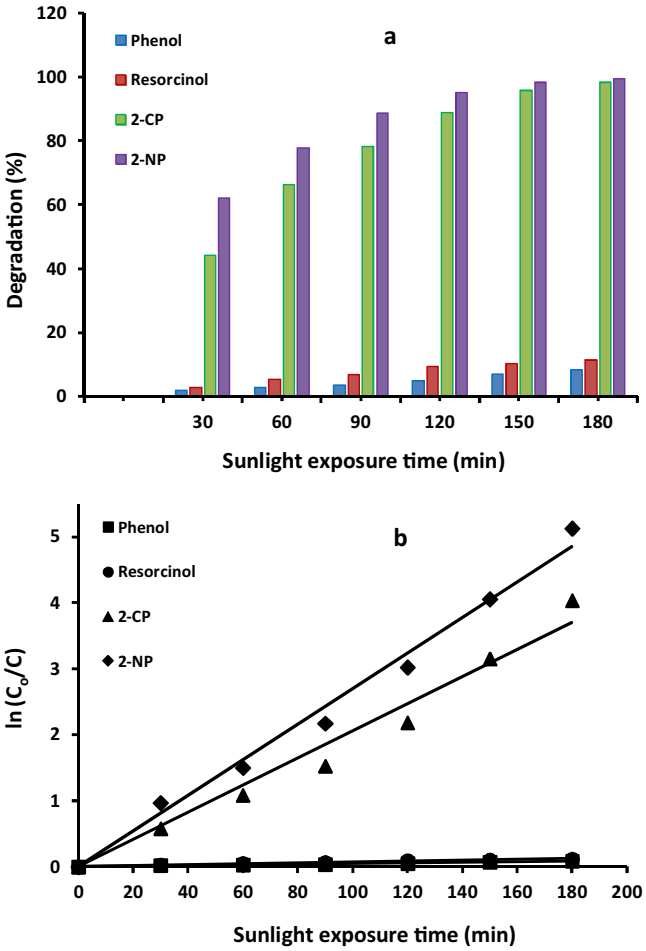

Fig. 5. The comparison of (a) time-scale percentage degradation of phenol and its derivatives evaluated from HPLC profiles (b) the graphical evaluation of rate constants for the degradation phenol and its derivatives in sunlight exposure at the catalyst loading of 300 mg suspended in 150 ml (30 ppm) of the respective phenol solution.

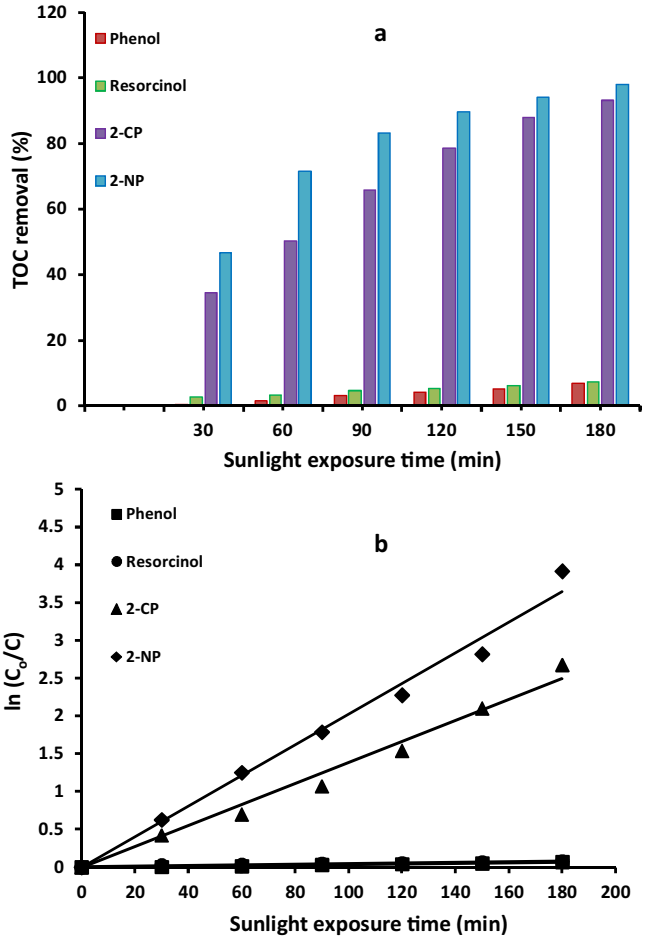

Fig. 6. The comparison of (a) time-scale percentage TOC removal of phenol and its derivatives (s) (b) the graphical evaluation of rate constants for the TOC removal of various phenolic substrates in sunlight exposure at the catalyst loading of 300 mg suspended in 150 ml (30 ppm) of respective phenol solution.

the absorption of photons having energy higher than the bandgap of WO_3, weakens the tungsten-oxygen bond that results in the creation of defect sites as presented in the equation below.

$$O-W^{6+}-O(2p)-W^{6+}-O+h\nu \rightarrow O-W^{5+}O^{-}(2p)-W^{6+}-O$$

$$W^{6+}O_3+h\nu \rightarrow W_x^{5+}W_{1-x}^{6+}O_3$$

The formation of defects composed of W^{5+} states not only imparts the greenish appearance, but also serves as electron trap centers. Among the oxidation states of tungsten, 4+ and 6+ oxidation states are regarded as more stable. The 4+ and 6+ oxidation states are stabilized by the unpaired electrons in 5d orbital and the hybridization of 5d and 6s orbits. Therefore, It is proposed that these photogenerated defects composed of W^{5+} states are responsible for the generation of $O_2^{\bullet-}$ anions even in the absence of suitable conduction band edge. The W^{5+} states, being short lives due to electronic considerations, facilitate the disbursement of electrons to O_2 to form superoxide anion radicals following a pathway similar to that proposed for TiO_2 [48]. The plausible mechanism is detailed below.

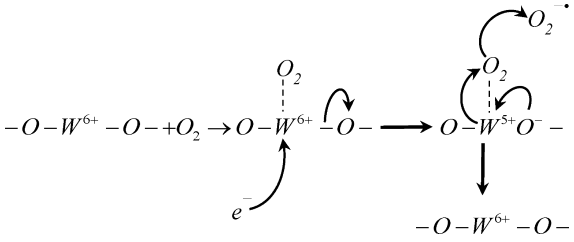

This effect was more pronounced in the complete spectrum of the sunlight as a significant decrease in the degradation and mineralization of 2-NP was observed in the visible portion of the sunlight. This observation led to the conclusion that the population of W^{5+} based defects is strongly dependant on photon energy and pronounced with the absorption of UV photons of sunlight.

As the mobility of superoxide anion radicals is well reported [49], it can be speculated that $O_2^{\bullet-}$ radicals, immediately after formation, leave the surface of WO_3 and diffused into the bulk. To verify the dependence of superoxide formation on the pH during photocatalytic degradation processes, the changes in pH during the course of the reaction were measured and presented in Fig. 7. For all the substrates, the variation of pH from 5.5 to 7.5 supports the formation and existence of superoxide anion radicals. The comparison of the degradation behavior of phenolic substrates

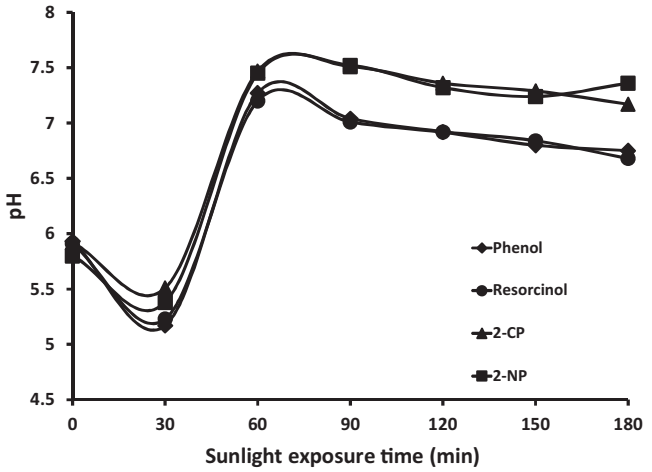

Fig. 7. The comparison of pH changes during the degradation of various phenolic substrates in sunlight exposure at the catalyst loading of 300 mg suspended in 150 ml (30 ppm) of the respective phenol solution.

(HPLC degradation and TOC removal profiles) also suggests the involvement of charged reactive species like $O_2^{\bullet-}$ in the degradation and removal process rather than hydroxyl radicals.

As evident from HPLC degradation profiles of all the substrates, the interaction of superoxide anion radicals, being charged in nature, is selective towards phenol and its derivatives. Possibly, the nature of the substituent attached to the aromatic system play a vital role in the degradation process. In the aqueous medium, phenol and its derivatives dissociate to H^+ along and phenoxide anions. The delocalization of excessive negative generated due to the release of H^+ ions on the aromatic ring is the dominant source of stabilization for phenoxide anions.

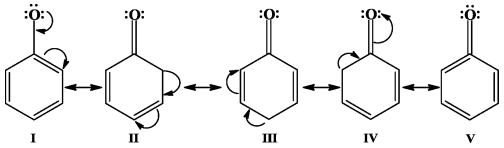

As demonstrated in the resonance structures above, the delocalization imparts excessive electrons to the aromatic ring, generating the negatively charged active sites that can facilitates the electrophilic attack only [50] while, in aqueous phase photocatalytic processes either negatively charged or neutral radical species are generated. As per experimental evidences based on HPLC/TOC profiles and the identification of the intermediates by GC–MS, it can be approximated that negatively charged $O_2^{\bullet-}$ are the major contributor both in degradation and mineralization process which signifies the nucleophilic interactions rather than electrophilic. This fact emphasizes the vital role of the substituents attached to the phenolic structure initially in the degradation process (loss of aromaticity) and finally in the mineralization process. This is well established that the presence of substituents on the ring either enhances or reduces the magnitude of negative charge on the ring by inductive effect. The extent of the inductive effect depends on the nature and arrangement of the constituent atoms that imparts "electron-withdrawing" and "electron-donating" property to the substituents. Electron-donating groups enhance the magnitude of negative charge on the aromatic ring by contributing the electrons (+I) while electron-withdrawing groups reduce it by –I effect. However in both the cases an overall negative charge sustain on the ring. Another interesting feature of the electron-withdrawing groups, being composed of electronegative atoms, is the induction of localized partial positive charge on the attached carbon atom. This effect is observable due to the distortion of the electronic cloud from

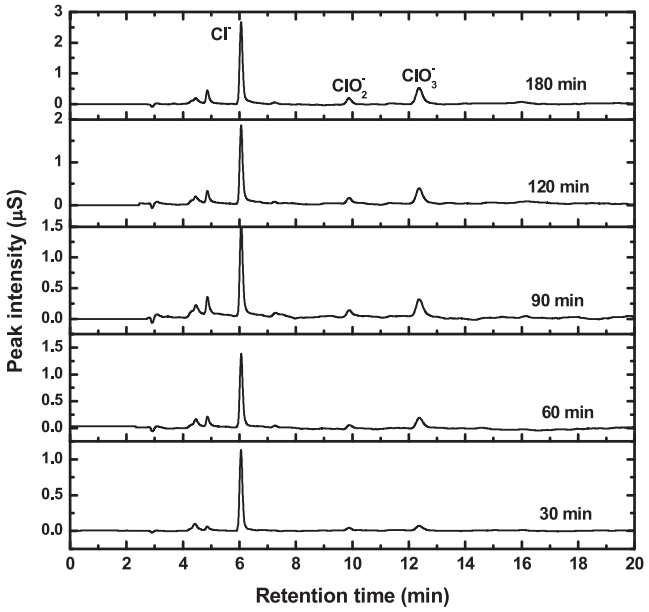

Fig. 8. The comparison of IC profiles for the release of Cl^-, ClO_2^- and ClO_3^- ions in the solution, at regular intervals, during the degradation of 2-chlorophenol in sunlight exposure at the catalyst loading of 300 mg of synthesized disc shaped WO_3 suspended in 150 ml (30 ppm) of 2-chlorophenol solution.

the attaching carbon atom towards the electronegative atoms. The presence of the partial positive charge on the electron-withdrawing group bearing carbon atom provides the interaction point to the attacking $O_2^{\bullet-}$ radicals causing the displacement of the electron-withdrawing groups that results in the loss of aromaticity thus degrading the phenol substrate. Unlike SN2 mechanism, the interaction of $O_2^{\bullet-}$ radicals not only displace the electron-withdrawing groups as negatively charged anions but also cleave the aromatic system leading to oxygenated intermediates. On the other hand, the electron donating groups being composed of less electronegative groups fail to induce such type of charge separation that results in the accumulation of excess negative charge on the ring. Phenol and resorcinol lack the property of inducing charge separation thus a low degradation was observed due the non-availability of active sites for $O_2^{\bullet-}$ attack. On the other hand, the charge separation in 2-CP and 2-NP facilitates the degradation process. The high degradation rate of 2-NP compared to 2-CP also confirms higher liability of NO_2 than Cl group.

The time-scale release of Cl^- ions, as measured by ion chromatography, in the solution during the photocatalytic degradation of 2-CP (Fig. 8) further strengthen the view that the degradation of phenol derivatives, with electron-withdrawing ability, is initiated by the displacement of the respective group by the $O_2^{\bullet-}$ radicals. Because of $O_2^{\bullet-}$ interaction the ring opening occurs with the formation of aliphatic oxygenates. The formation of ClO_2^- and ClO_3^- was also observed which depicts the further interaction of Cl^- with either dissolved oxygen $O_2^{\bullet-}$ radicals or other reactive species however, in the presence of a variety of charged and radical species generated it is hard to estimate the exact mechanism for their formation. The comparison of the release of chloride and chlorate with the increasing sunlight exposure time is presented in Fig. 9. The degradation of 2-NP was interesting as a low concentration of both NO_2 and NO_3 anions was observed (Fig. 10) while HPLC and TOC confirmed the degradation and mineralization rate even higher than 2-CP. This observation pointed towards the conversion of NO_2^- ions to NO_3^- and NH_4^+ ions. The presence of NH_4^+ ions in IC analysis indicated the conversion of NO_2^- to NH_4^+ ions that can be a possible cause for the low concentration of NO_2^- ions in the

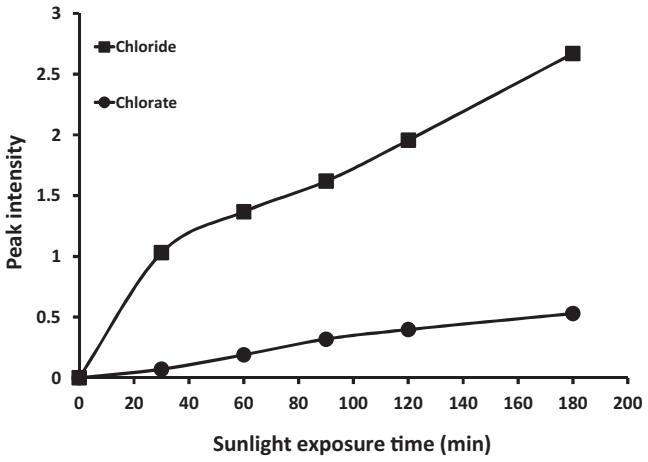

Fig. 9. The comparison of time-scale changes in the concentration of Cl^- and ClO_3^- during the degradation of 2-chlorophenol in sunlight exposure at the catalyst loading of 300 mg of synthesized disc shaped WO_3 suspended in 150 ml (30 ppm) of 2-chlorophenol solution.

solution. Another possibility, as presented in Eq. (13), is the release of NO_2^- in the form of NO_2 gas after donating the excess negative charge to photogenerated holes.

$$NO_2^- + h^+ \rightarrow NO_2 \uparrow \quad (13)$$

It has also been reported that once formed, in the aqueous medium, NO_2 gas can undergo a variety of reactions [51]. The possible reactions are detailed below.

$$NO_2 + NO_2 \rightarrow N_2O_4 \quad (14)$$

$$NO_2 + NO_2^- \rightarrow NO_3^- + NO \quad (15)$$

$$N_2O_4 + H_2O \rightarrow NO_3^- + H^+ + HNO_2 \quad (16)$$

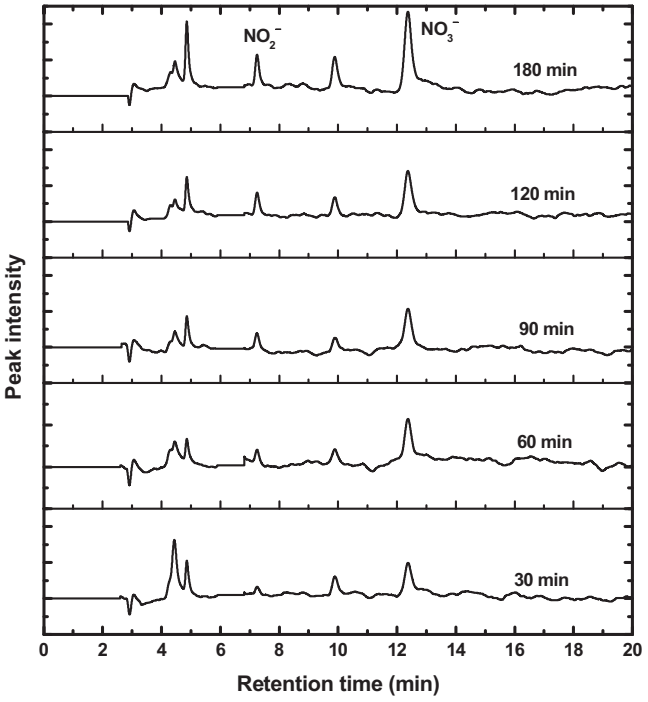

Fig. 10. The comparison of IC profiles for the release of NO_2^- and NO_3^- ions in the solution, at regular intervals, during the degradation of 2-nitrophenol in sunlight exposure at the catalyst loading of 300 mg of synthesized disc shaped WO_3 suspended in 150 ml (30 ppm) of 2-nitrophenol solution.

The occurring of above mentioned reactions (Eqs. (14)–(16)) validates the formation of NO_2 gas through the oxidation of nitrite ions by the photogenerated holes (Eq. (13)) that results in the low concentration of nitrite ions in the solution. Although in very low concentration, the identification of resorcinol and poly-hydroxy phenols in the degradation of phenol and resorcinol respectively, also confirmed by HPLC, indicated the involvement of hydroxyl radicals in the degradation process. As presented in the reaction below, the only possible route for the formation of resorcinol from phenol and poly-hydroxy phenol is the interaction of hydroxyl radicals with phenol and resorcinol.

A similar situation was observed for the degradation of resorcinol. Based on this observation, it can be assumed that the hydroxylated intermediates are also formed in the degradation of 2-CP and 2-NP, but degraded/mineralized instantaneously after formation. Therefore, the formation of hydroxyl radicals in the aqueous photocatalytic processes cannot be completely ignored. Nonetheless, the low degradation of phenol and the formation of resorcinol in significantly lower concentration, as intermediate, clearly question their role as the major oxidizing species. Although in very low concentration, the other products identified in the degradation of phenol and resorcinol are listed below.

In the GC–MS identification of intermediates for the degradation of 2-CP and 2-NP, no aromatic compound other than the substrates was identified. Almost similar products, mostly aliphatic oxygenates, were identified in the degradation of both 2-CP and 2-NP. However, a higher concentration of intermediates for 2-CP compared to 2-NP was observed. The identified major intermediates for 2-CP and 2-NP degradation are detailed below.

The non-existence of any aromatic intermediate and the identification of oxygenated intermediates postulate that the degradation of 2-CP and 2NP is initiated by the displacement of Cl and NO_2 groups and ring opening simultaneously. The oxygen after displacing the respective anions is incorporated in the chain. The presence of electronegative oxygen atoms induces charge separation, hence generating additional targets for $O_2^{\bullet-}$ attack. The interaction of $O_2^{\bullet-}$ radicals with the oxygenated intermediates initiates both the mineralization and fragmentation simultaneously. The identification of the variety of C1-C5 products supports that the fragmentation and mineralization proceed simultaneously.

A marked decrease ($\sim$ 50%) in the activity of the WO_3 discs was observed in the visible region (400–800 nm) of sunlight which led to the conclusion that the increasing energy of the incident photons facilitates the generation of W^{5+} states that in turn enhances the production of superoxide ($O_2^{\bullet-}$) anions. The WO_3 discs showed excellent activity in repeated use without significant decrease in degradation ability.

4. Conclusions

The study proved that by controlling the morphology of the photocatalysts the photocatalytic activity can be enhanced. Although, based on the potential of conduction band edge, WO_3 is unable to produce superoxide anions however, $O_2^{\bullet-}$ radicals are produced by alternative mechanism and contribute as major oxidizing species in the oxidation of phenols and its derivatives. The presence of electron withdrawing substituents facilitates the degradation and mineralization of aromatic structure, whereas electron donating groups retard the same. The generation of hydroxyl groups in photocatalytic processes and their contribution in the degradation process cannot be negated completely however the overall contribution is minor as compared to that of superoxide anions. The degradation of phenol derivatives with electron-withdrawing groups proceed through ring opening and

fragmentation. The fragments are further interacted by the oxidizing species to mineralization.

Acknowledgments

Authors are greatly indebted to the Center of Excellence and Environmental Studies (CEES), King Abdulaziz University and Ministry of Higher Education (MoHE), Kingdom of Saudi Arabia, for their supports.

References

[1] Y. Zhang, D. Ma, Y. Zhang, W. Chen, S. Huang, N-doped carbon quantum dots for TiO_2-based photocatalysts and dye-sensitized solar cells, Nano Energy 2 (2013) 545–552.
[2] Y. Kondo, H. Yoshikawa, K. Awaga, M. Murayama, T. Mori, K. Sunada, S. Bandow, S. Iijima, Preparation, photocatalytic activities, and dye-sensitized solar- cell performance of submicron-scale TiO_2 hollow spheres, Langmuir 24 (2008) 547–550.
[3] C. Shifu, C. Gengyu, Photocatalytic degradation of organophosphorus pesticides using floating photocatalyst $TiO_2{\cdot}SiO_2$/beads by sunlight, Sol. Energy 79 (2005) 1–9.
[4] M. Sharon, B. Pal, D.V. Kamat, Photocatalytic killing of pathogenic bacterial cells using nanosize Fe_2O_3 and carbon nanotubes, J. Biomed. Nanotechnol. 1 (2005) 365–368.
[5] M. Canle, M.I. Fernandez, S. Rodriguez, J.A. Santaballa, S. Steenken, E. Vulliet, Mechanisms of direct and TiO_2-photocatalysed UV degradation of phenylurea herbicides, ChemPhysChem 6 (2005) 2064–2074.
[6] M. Miyauchi, Photocatalysis and photoinduced hydrophilicity of WO_3 thin films with underlying Pt nanoparticles, Phys. Chem. Chem. Phys. 10 (2008) 6258–6265.
[7] M.H. Hernández-Alonso, F. Fresno, S. Suárez, J.M. Coronado, Development of alternative photocatalysts to TiO_2: challenges and opportunities, Energy Environ. Sci. 2 (2009) 1231–1257.
[8] S. Rehman, R. Ullah, A.M. Butt, N.D. Gohar, Strategies of making TiO_2 and ZnO visible light active, J. Hazard. Mater. 170 (2009) 560–5699.
[9] A. Fujishima, T.N. Rao, D.A. Tryk, Titanium dioxide photocatalysis, J. Photochem. Photobiol., C: Photochem. Rev. 1 (2000) 1–21.
[10] Q.U. Jiuhui, Research progress of novel adsorption processes in water purification: a review, J. Environ. Sci. 20 (2008) 1–13.
[11] D.S. Bhatkhande, V.G. Pangarkar, A.A.C.M. Beenackers, Photocatalytic degradation for environmental applications—a review, J. Chem. Technol. Biotechnol. 77 (2002) 102–116.
[12] C. Lettmann, H. Hinrichs, W.F. Maier, Combinatorial discovery of new photocatalysts for water purification with visible light, Angew. Chem. Int. Ed. 40 (2001) 3160–3164.
[13] M.A. Lazar, S. Varghese, S.S. Nair, Photocatalytic water treatment by titanium dioxide: recent updates, Catalysts 2 (2012) 572–601.
[14] A. Mills, R.H. Davies, D. Worsley, Water-purification by semiconductor photocatalysis, Chem. Soc. Rev. 22 (1993) 417–425.
[15] M.N. Chong, B. Jin, C.W.K. Chow, C. Saint, Recent developments in photocatalytic water treatment technology: a review, Water Res. 44 (2010) 2997–3027.
[16] A. Mills, S. Le Hunte, An overview of semiconductor photocatalysis, J. Photochem. Photobiol., A: Chem. 108 (1997) 1–35.
[17] D.F. Ollis, E. Pelizzetti, N. Serpone, Photocatalyzed destruction of water contaminants, Environ. Sci. Technol. 25 (1991) 1522–1529.
[18] M.R. Hoffmann, S. Martin, W. Choi, D.W. Bahnemann, Environmental applications of semiconductor photocatalysis, Chem. Rev. 95 (1995) 69–96.
[19] R. Andreozzi, V. Caprio, A. Insola, R. Marotta, Advanced oxidation processes (AOP) for water purification and recovery, Catal. Today 53 (1999) 51–59.
[20] D.A. Tryk, A. Fujishima, K. Honda, Recent topics in photoelectrochemistry: achievements and future prospects, Electrochim. Acta 45 (2000) 2363–2376.
[21] M. Kositzi, I. Poulios, S. Malato, J. Caceres, A. Campos, Solar photocatalytic treatment of synthetic municipal wastewater, Water Res. 38 (2004) 1147–1154.
[22] S. Malato, P. Fernández-Ibáñez, M.I. Maldonado, J. Blanco, W. Gernjak, Decontamination and disinfection of water by solar photocatalysis: recent overview and trends, Catal. Today 147 (2009) 1–59.
[23] D. Bahnemann, Photocatalytic water treatment: solar energy applications, Sol. Energy 77 (2004) 445–459.
[24] S. Chakrabarti, B.K. Dutta, Photocatalytic degradation of model textile dyes in wastewater using ZnO as semiconductor catalyst, J. Hazard. Mater. 112 (2004) 269–278.
[25] J.N. Daneshvar, D. Salari, A.R. Khataee, Photocatalytic degradation of azo dye acid red 14 in water on ZnO as an alternative catalyst to TiO_2, J. Photochem. Photobiol., A: Chem. 162 (2004) 317–322.
[26] S.K. Kansal, A.H. Ali, S. Kapoor, Photocatalytic decolorization of beibrich scarlet dye in aqueous phase using different nanophotocatalysts, Desalination 259 (2010) 147–155.
[27] R. Velmurugan, M. Swaminathan, An efficient nanostructured ZnO for dye sensitized degradation of Reactive Red 120 dye under solar light, Sol. Energy Mater. Sol. Cells 95 (2011) 942–950.
[28] G.R. Bamwenda, H. Arakawa, The visible light induced photocatalytic activity of tungsten trioxide powders, Appl. Catal., A: Gen. 210 (2001) 181–191.
[29] Z.G. Zhao, M. Miyauchi, Nanoporous-walled tungsten oxide nanotubes as highly active visible-light-driven photocatalysts, Angew. Chem. Int. Ed. 47 (2008) 7051–7055.
[30] R.Q. Cabrera, E.R. Latimer, A. Kafizas, C.S. Blackman, C.J. Carmalt, I.P. Parkin, Photocatalytic activity of needle-like TiO_2/WO_{3-x} thin films prepared by chemical vapour deposition, J. Photochem. Photobiol., A: Chem. 239 (2012) 60–64.
[31] D. Li, H. Haneda, Morphologies of zinc oxide particles and their effects on photocatalysis, Chemosphere 51 (2003) 129–137.
[32] J. Yu, L. Qi, Template-free fabrication of hierarchically flower-like tungsten trioxide assemblies with enhanced visible-light-driven photocatalytic activity, J Hazard. Mater. 169 (2009) 221–227.
[33] A. Wolcott, T.R. Kuykendall, W. Chen, S. Chen, J.Z. Zhang, Synthesis and characterization of ultrathin WO_3 nanodisks utilizing long-chain poly(ethylene glycol), J. Phys. Chem. B 110 (2006) 25288–25296.
[34] M. Czaplicka, Sources and transformations of chlorophenols in the natural environment, Sci. Total Environ. 322 (2004) 21–39.
[35] U.S. Environmental Protection Agency, Ambient Water Quality Criteria for Nitrophenols, U.S. Environmental Protection Agency, Washington, DC, 1980.
[36] S.S. Adav, M.Y. Chen, D.J. Lee, N.Q. Ren, Degradation of phenol by Acinetobacter strain isolated from aerobic granules, Chemosphere 67 (2007) 1566–1572.
[37] N. Calace, E. Nardi, B.M. Petronio, M. Pietroletti, Adsorption of phenols by paper mill sludge, Environ. Pollut. 118 (2002) 315–319.
[38] F.A. Carey, Organic Chemistry, fourth ed., McGraw-Hill, New York, NY, 2000, pp. 945.
[39] O.A. O'Connor, L.Y. Young, Toxicity and anaerobic biodegradibility of substituted phenols under methanogenic conditions, Environ. Toxicol. Chem. 8 (1989) 853–862.
[40] U.I. Gaya, A.H. Abdullah, Heterogeneous photocatalytic degradation of organic contaminants over titanium dioxide: A review of fundamentals, progress and problems, J. Photochem. Photobiol., C: Photochem. Rev. 9 (2008) 1–12.
[41] P. Pichat, Photocatalysis and Water Purification from Fundamentals to Recent Applications, firsst ed., Wiley-VCH Verlag, GmBH Germany, 2013.
[42] M.A. Gondal, A. Hameed, A. Suwaiyan, Photo-catalytic conversion of methane into methanol using visible laser, Appl. Catal., A: Gen. 243 (2003) 165–174.
[43] M.A. Gondal, A. Hameed, Z.H. Yamani, A. Arfaj, Photocatalytic transformation of methane into methanol under UV laser irradiation over WO_3, TiO_2 and NiO catalysts, Chem. Phys. Lett. 392 (2004) 372–377.
[44] M.A. Gondal, A. Hameed, Z.H. Yamani, Laser induced photocatalytic splitting of water over WO_3 catalyst, Energy Sources 27 (2005) 1151–1165.
[45] A. Hameed, I.M.I. Ismail, M. Aslam, M.A. Gondal, Photocatalytic conversion of methane into methanol: Performance of silver impregnated WO_3, Appl. Catal., A: Gen. 470 (2014) 327–335.
[46] N. Xu, M. Sun, Y.W. Cao, J.N. Yao, E.G. Wang, Influence of pH on structure and photochromic behavior of nanocrystalline WO_3 films, Appl. Surf. Sci. 157 (2000) 81–84.
[47] T. Arai, M. Horiguchi, M. Yanagida, T. Gunji, H. Sugihara, K. Sayama, Complete oxidation of acetaldehyde and toluene over a Pd/WO_3 photocatalyst under fluorescent- or visible-light irradiation, Chem. Commun. 43 (2008) 5565–5567.
[48] R. Nakamura, A. Imanishi, K. Murakoshi, Y. Nakato, In situ FTIR studies of primary intermediates of photocatalytic reactions on nanocrystalline TiO_2 films in contact with aqueous solutions, J. Am. Chem. Soc. 125 (2003) 7443–7450.
[49] B.G. Kwon, J. Yoon, Mobility of $HO^{\bullet}/O_2^{-\bullet}$ generated from TiO_2 photocatalysis, Bull. Korean Chem. Soc. 30 (2009) 667–670.
[50] M.B. Smith, March's Advanced Organic Chemistry: Reactions, Mechanisms, and Structure, seventh ed., Wiley, New York, 2013.
[51] T.L. Broder, D.S. Silvester, L. Aldous, C. Hardacre, R.G. Compton, Electrochemical oxidation of nitrite and the oxidation and reduction of NO_2 in the room temperature ionic liquid [C2mim][NTf2], J. Phys. Chem. B 111 (2007) 7778–7785.